CIVIL ENGINEERING JOURNAL

Article no. 2

THE CIVIL ENGINEERING JOURNAL 1-2026

NEGATIVE MOMENT ZONE IN UHPC-STRENGTHENED SIMPLY-SUPPORTED-TO-CONTINUOUS CONCRETE BOX BEAMS: CRACKING RESISTANCE ANALYSIS

Junming Huang[1], Kexin Zhang[2] and Jiaqi Qiu[2]

1. *School of Management, Shenyang Jianzhu University, Shenyang, No.25 Hunnan Zhong Road, China; 2423805749@qq.com*
2. *School of Transportation and Geomatics Engineering, Shenyang Jianzhu University, Shenyang, No.25 Hunnan Zhong Road, China; jt_zkx@sjzu.edu.cn*

Received: *28.05.2025*

Received in revised form: *21.01.2026*

Accepted: *19.03.2026*

ABSTRACT

In this study, to investigate the cracking resistance of UHPC-strengthened simply-supported-to-continuous concrete box beams in the negative moment zone, a total of nine specimens were designed: one reinforced concrete box beam (comparison beam), seven UHPC-RC composite box beams (reinforced beams), and one prestressed concrete box beam (prestressed beam). The research focuses on evaluating the influence of key parameters - including reinforcement ratio, UHPC casting length in the negative moment zone, UHPC thickness, and the joint configuration between UHPC and ordinary concrete - on the cracking resistance of these beams. The results demonstrate that, under the same reinforcement ratio, UHPC strengthening in the negative moment zone significantly enhances the cracking performance of the test beams, with the cracking load increasing by 46%. As the UHPC casting length increases, the maximum crack width at the vertical interface between the full normal concrete (NC) section and the UHPC-NC composite section decreases markedly. Additionally, increasing the UHPC thickness leads to a substantial reduction in the maximum crack width at both the UHPC-NC composite section and the intermediate diaphragm section.

KEYWORDS

Simply-supported to continuous concrete box beam, Negative moment zone, UHPC, Cracking resistance

INTRODUCTION

Simply-supported to continuous beam bridge has been widely used in highway construction by virtue of its advantages of simple structure, high degree of assembly, low cost and fast construction speed [1-2]. Accompanied by the rapid development of the economy, the pressure of highway traffic is also gradually increased, the simply-supported to continuous beam bridge of some problems have begun to appear [3-5], which in turn to the top of the abutment negative bending moment region of the problem is most prominent. Due to the low tensile strength of ordinary concrete and insufficient crack resistance, cracks are produced in the negative moment region at the top of the abutment of simply-supported to continuous concrete beam bridges, which seriously affects the durability and normal service life of the bridge [6]. Therefore, improving the crack resistance in the

negative moment zone of simply-supported to continuous beam bridges to improve the durability of bridge operation has become the focus of research [7-8].

The traditional mechanical tensioning prestressing method is to limit the crack development in the negative moment zone by tensioning the prestressing bundles in the negative moment zone at the top of the pier [9]. The crack resistance of the beams is improved by applying prestressing to the negative moment region of the combined beams, but its construction is complicated, inefficient, costly and difficult to ensure the construction quality [10-13]. Therefore, it aims to solve the cracking problem in the negative moment zone of simply-supported to continuous beam bridges, and on this basis, effectively improve the construction efficiency and reduce the construction difficulty and cost.

In recent years, with the vigorous development of material science, many new materials have emerged to provide new solutions to the cracking problem in the negative moment region of beam bridges. Ultra-High Performance Concrete (UHPC), as a new type of cementitious composite material, has the characteristics of ultra-high strength, high toughness, and high durability, and its compressive strength can reach more than 150 MPa and tensile strength can reach more than 6 MPa [14-17]. Long G. [18] carried out a study on UHPC-RC combination beams, and analysed in-depth the effect of the thickness of UHPC on the crack resistance of bridges as well as the ultimate load carrying capacity. Liu X. [19] conducted a study on UHPC-steel composite beams and analysed in-depth the influence of UHPC on improving the crack resistance of composite beams. Wan Z. [20] conducted a study on UHPC-steel-concrete composite beams and analysed in-depth the influence of several parameters, such as the type of overlaying concrete, the arrangement of interfacial shear reinforcement, and the presence of steel wire mesh, on the structural performance of the added composite beams. At present, the research on the structural aspects of UHPC mainly focuses on the combined beams, while there are few studies on the negative moment region of UHPC-strengthened simply-supported to continuous structures.

To address the cracking issue in the negative moment zone of simply-supported-to-continuous beam bridges, this study innovatively applies UHPC to the negative moment zone of simply-supported-to-continuous concrete box beams, forming a locally UHPC-strengthened structural system. This approach effectively mitigates cracking in the negative moment zone. Owing to UHPC's superior tensile properties, it replaces the conventional bridge system conversion method, which involves “pouring concrete over the pier continuous section (at the joint) + mechanically tensioned prestressing.” This innovation not only enhances construction efficiency but also reduces associated risks. Although UHPC materials are more expensive than ordinary concrete, their exceptional performance and durability significantly lower long-term maintenance costs, ensuring economic viability over the service life of the structure. This paper investigates the structural behavior of such composite box beams by considering variables including reinforcement ratio, UHPC length and thickness, prestressing tendon arrangement, and the presence of bearers. The findings provide a theoretical foundation for the practical application of this innovative beam type.

TEST PROCEDURE

Materials

Mechanical Properties of Ordinary Concrete

The grade of plain concrete used is C40 and the specific mix is shown in Table 1.

Tab. 1 - C40 concrete mix

Material	Quality ratio (kg/m^3)
Water	0.33
cement	1
sand	1.15
cobble	2.26
Water reducing agent	0.004

In order to determine the specific mechanical properties of the C40 concrete used in the test beams, three cubic specimens of 150 mm × 150 mm × 150 mm, three prismatic specimens of 100 mm × 100 mm × 400 mm, and three prismatic specimens of 100 mm × 100 mm × 300 mm were poured and cast, and the tests of compressive strength, flexural strength, and modulus of elasticity were carried out respectively. The specimens were all poured at the same time as the concrete of the precast section of the test beam, and the curing was completed under the same conditions. The tests were carried out in accordance with the standard test methods in the Standard Test Methods for Concrete Structures (GB/T 50152-2012), and the average values of the basic mechanical properties of each group of specimens are shown in Table 2.

Tab. 2 - C40 concrete mix

Concrete type	Cubic compressive strength（MPa）	Flexural strength（MPa）	Modulus of elasticity（MPa）
C40	40.9	2.47	26500

Mechanical Properties of UHPC

The UHPC matrix was doped with steel fibers of end-hook type at a dosage of 2% and the specific mixing ratios are shown in Table 3.

Tab. 3 - UHPC material mix ratios

Composition	Quality ratio (kg/m^3)
Cement	956
Medium Sand	214.2
Fine Sand	856.8
Silica Fume	159
Quartz Powder	159
Water Reducing Agent	25.5
Water	216.7

With reference to the specification “Activated Powder Concrete” (GB 50010-2010), three 100 mm × 100 mm × 100 mm cubic compression specimens, three 100 mm × 100 mm × 400 mm prismatic flexural specimens, and three dumbbell-shaped tensile specimens were cast to test the compressive and flexural strengths and tensile strengths of the UHPC. The specimens were cast in the same batch with the test beams, and the maintenance was completed under the same conditions, and the average values of the material performance test results are shown in Table 4, and the axial tensile diagram is shown in Figure 1.

Fig. 1 – Tensile strength test

Tab. 4 - UHPC mechanical properties test results

Cubic compressive strength（MPa）	Flexural strength（MPa）	Tensile strength（MPa）
122	23.3	7.91

Mechanical properties of steel bars

The tensile steel bars used in the test are HRB400 grade, and the pull-out test is carried out to test the yield strength and ultimate tensile strength of the steel bars, and the mechanical properties of the steel bars are shown in Table 5.

Tab. 5 - Test results of mechanical properties of reinforcing steel

Reinforcement diameter（mm）	Modulus of elasticity（MPa）	Yield strength（MPa）	Ultimate tensile strength（MPa）
10	2.0×10^5	422	578
12	2.0×10^5	428	587
14	2.0×10^5	437	592

Test Beam Design and Casting Process

The main steps for making the test beam are as follows: reinforcement cage tying, concrete material preparation, concrete pouring, cast-in-place section reinforcement tying, concrete pouring for end beams as well as beams in the negative moment zone, UHPC pouring in the negative moment zone, formwork dismantling, and maintenance of the test beam. The steps of box beam casting are shown in Figure 2.

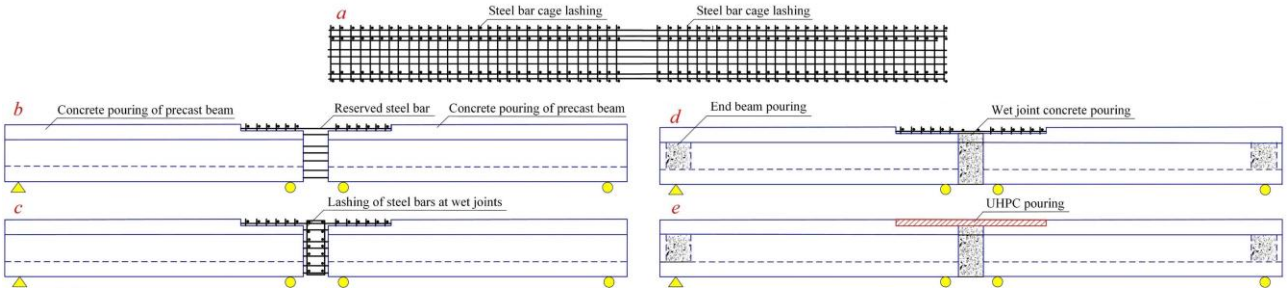

Fig. 2 – Schematic diagram of UHPC reinforced simply-supported to continuous concrete box beams in negative moment zone: (a) – precast beams reinforcement cage tying; (b) – precast beams concrete pouring; (c) – wet joints reinforcement tying; (d) – wet joints and end beams concrete pouring; (e) – UHPC pouring.

Site Pouring Process

The fabrication process of box beams is depicted in Figure 3, primarily involving two main steps: the construction of formwork and the tying of reinforcement cages, followed by the pouring of both conventional concrete materials and UHPC.

Formwork Production and Reinforcement Cage Tying

After the completion of the template production, in accordance with the design drawings of the size of the rebar and the location of the cage will be tied, the rebar between the use of fine steel wire bonding, the test of the reinforcing steel used for the HRB400 level, to be strain gauges paste can be poured, the template and the cage as shown in Figure 3 (a).

Pouring of Concrete Materials

Prepare the concrete mixture, and then slowly pour it into the formwork. During the pouring process, continuously vibrate the concrete using a vibrator to ensure it is uniformly distributed and compacted. After allowing the poured concrete to set for approximately 2 h, smooth the concrete surface again with a trowel. To minimize water loss and prevent cracking after the concrete has been poured, cover the surface with cling film after sprinkling it with water, and regularly moisten the surface thereafter. After about 7 d of curing, concrete can be poured for the end beams as well as the beams in the negative moment region. The specific pouring process is illustrated in Figure 3(b) and Figure 3(c).

UHPC Pouring

After the curing of the plain concrete region was finished, the UHPC-NC interface was chiseled using a chisel hammer. During the chiseling process, efforts were made to partially expose the coarse aggregate on the surface. Once chiseling was complete, any debris on the chiseled surface was cleaned off using an air pump. Subsequently, the UHPC material was prepared and poured into the negative moment zone of the box beam. Given that UHPC possesses self-compacting and self-leveling properties, it was not necessary to use vibrating instruments during the pouring process. After pouring, the surface was smoothed with a trowel and then covered with a plastic film to prevent moisture loss. The formwork was removed, and the structure was allowed to cure at room temperature for 28 d before testing. The UHPC pouring and curing process is illustrated in Figures 3(d) to 3(f).

Fig. 3 – Box beam fabrication process: (a) – supporting formwork and tying reinforcement, (b) – pouring precast concrete, (c) – pouring concrete for center diaphragm, (d) – mixing UHPC, (e) – pouring UHPC, and (f) – curing after UHPC pouring

Test Procedure

Taking the length of UHPC in the negative moment zone, the thickness of the UHPC layer, and the reinforcement ratio of ordinary steel as the primary variables, a total of nine test beams were designed for the experiment. Among these, one was a simply-supported-to-continuous ordinary reinforced concrete box beam, another was a simply-supported-to-continuous prestressed reinforced concrete box beam, and the remaining seven were simply-supported-to-continuous concrete box beams locally strengthened with UHPC. The parameters for each test beam are detailed in Table 6, while the specific dimensions of the test beams are illustrated in Figures 4 to 6.

Tab. 6 - Pilot programme

Test beam number	Length of UHPC L/mm	Plain steel reinforcement ratio（%）	Prestressing tendon	Thickness of UHPC /mm	Forms of Concrete Undertaking
B0	—	0.43	—	—	Groove
B1	1600	0.36	—	60	Groove
B2	1600	0.43	—	60	Groove
B3	1600	0.50	—	60	Groove
B4	800	0.43	—	60	Groove
B5	1200	0.43	—	60	Groove
B6	—	0.43	2Φs15.2	—	—
B7	1600	0.43	—	120	Bearing
B8	1600	0.43	—	120	Unsupported

The test beam has a longitudinal length of 5000 mm, a clear span of 4600 mm, and a beam height of 450 mm. The flange plate thickness is 120 mm, with a bottom plate width of 1200 mm and a top plate width of 700 mm. The concrete cover thickness is 20 mm, the ordinary concrete used has a strength grade of C40, and all ordinary reinforcing bars are of HRB400 grade. Additionally, cross beams with thicknesses of 300 mm and 200 mm are installed at both ends and the middle of the beam, respectively. In this experiment, key analysis factors include varying ordinary steel reinforcement ratios, UHPC casting lengths and thicknesses, as well as the interfacial bonding forms between ordinary concrete and UHPC.

Among the test beams, beams B1, B2, and B3 all featured a UHPC casting length of 1.6 meters, but they had different ordinary reinforcement ratios, specifically 0.36%, 0.43%, and 0.50%, respectively. Beams B2, B4, and B5 shared the same ordinary reinforcement ratio, yet their UHPC casting lengths varied, measuring 1.6 m, 0.8 m, and 1.2 m, respectively. For beam B6, based on the configuration of beam B0, two nominally symmetrical UHPC sections were arranged. The

thicknesses of the UHPC castings for beams B2, B7, and B8 were 60 mm, 120 mm, and 120 mm, respectively. Notably, the interface between UHPC and NC (normal concrete) for beam B7 utilized a bracket-supported bearing form, whereas for beam B8, it was without bracket support.

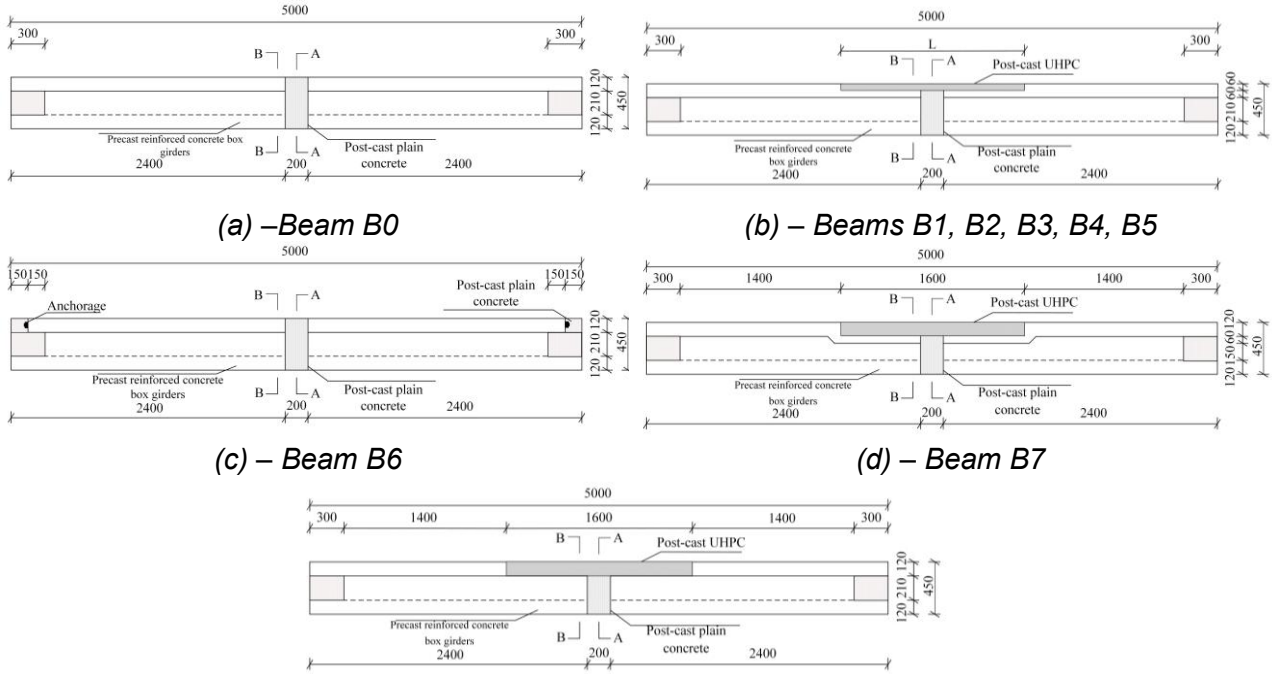

(a) –Beam B0

(b) – Beams B1, B2, B3, B4, B5

(c) – Beam B6

(d) – Beam B7

(e) – Beam B8

Fig. 4 – Elevation of test beam (unit: mm)

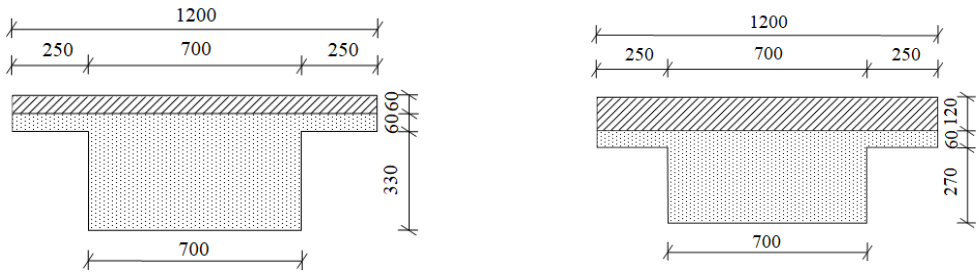

(a) – Beams B1, B2, B3, B4, B5

(b) –Beam B7

Fig. 5 – Section A-A of test beam (unit: mm)

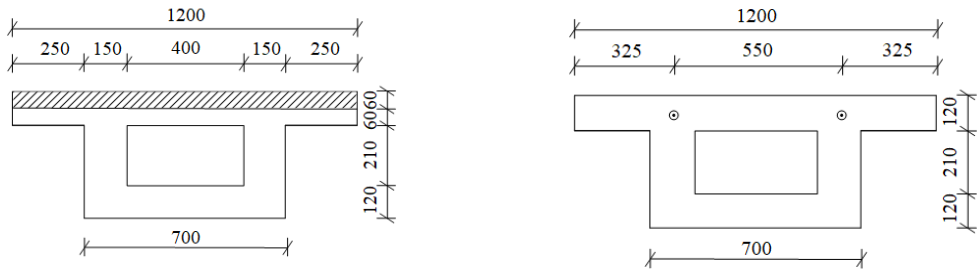

(a) – Beams B1, B2, B3, B4, B5

(b) – Beam B8

Fig. 6 – section B-B of test beam (unit: mm)

Load and Measurement Point Arrangement

The test beams were inverted, and reversed loading was employed to simulate the negative bending moment acting on the main beams. Loading was applied using 1000 kN hydraulic jacks, with the beam ends supported on steel piers spaced 4600 mm apart. The test was conducted with four loading points, and the distance between each loading point was set at 600 mm. Schematic diagrams of the loading setup for the test beams, along with on-site photographs, are presented in Figures 7 and 8.

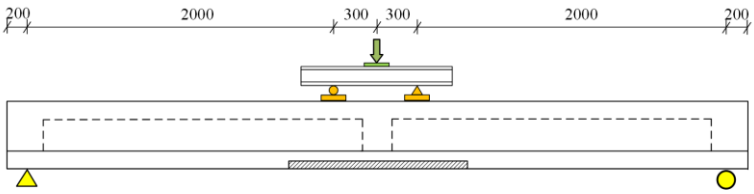

Fig. 7 – Schematic diagram of test loading (unit: mm)

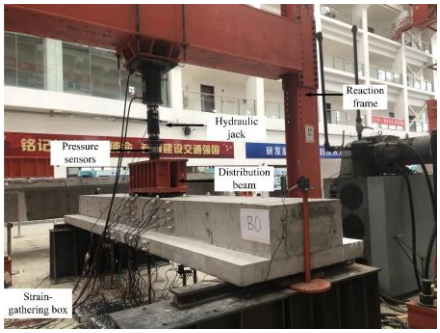

Fig. 8 –Pictures of the test site

RESULTS AND DISCUSSION

Effect of Crack Distribution Under Different Influencing Factors

Factors for Reinforcement Ratio of Ordinary Steel Bars

The simply-supported-to-continuous concrete box beam locally strengthened with UHPC is categorized into four distinct regions, as illustrated in Figure 9. Region Ⅰ represents the full normal concrete (NC) section located outside the UHPC-strengthened area; Region Ⅱ denotes the vertical interface between the combined UHPC-NC section and the full NC section; Region Ⅲ corresponds to the combined UHPC-NC section itself; and Region Ⅳ signifies the intermediate diaphragm beam section. The variations in maximum crack width with respect to applied load for each region in beams B1, B2, and B3 are depicted in Figure 10. Additionally, a comparative analysis of the load versus maximum crack width curves for each region across the test beams is presented in Figure 11.

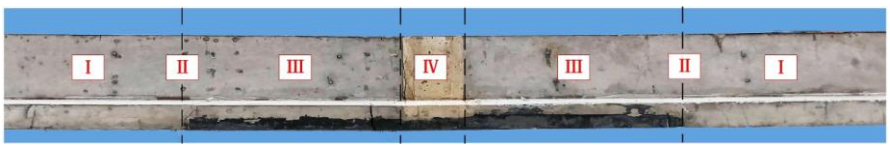

Fig. 9 – Map of the division of the test beam region (B2 beam)

As illustrated in Figure 10(a), when the external load reaches 85 kN, the first crack emerges in Region Ⅰ of beam B1, followed sequentially by cracks in Regions Ⅱ, Ⅳ, and Ⅲ. As the load increases, the maximum crack widths in all four regions—Ⅰ, Ⅱ, Ⅲ, and Ⅳ—generally exhibit a linear growth trend. When the load surpasses 200 kN, the stiffness of the UHPC-NC composite cross-section significantly decreases, leading to a relatively slower increase in crack width in Regions Ⅰ and Ⅱ, while the crack width in Region Ⅳ grows more rapidly. Ultimately, the beam fails at the intermediate diaphragm cross-section.

From Figure 10(b), it is evident that the first crack in beam B2 appears in Region Ⅰ when the load reaches 95 kN, followed by cracks in Regions Ⅱ, Ⅳ, and Ⅲ in sequence. When the load increases to approximately 120 kN, the crack width in Region Ⅰ is the first to reach 0.2 mm, followed by a crack width of 0.1 mm in Region Ⅱ, while cracks in Regions Ⅲ and Ⅳ have not yet appeared. As the load continues to rise, the maximum crack widths in all four regions—Ⅰ, Ⅱ, Ⅲ, and Ⅳ—generally show linear growth, albeit at a relatively slow rate. When the load exceeds 270 kN, some of the reinforcement in Region Ⅱ yields, causing the crack width there to increase sharply with further load increase.

From Figure 10(c), it can be observed that when beam B3 is loaded to 100 kN, cracks successively appear in Regions Ⅰ, Ⅱ, and Ⅳ, with widths of 0.02 mm, 0.1 mm, and 0.1 mm, respectively. Cracks in Region Ⅲ emerge when the external load reaches 120 kN, at which point the maximum crack width in Region Ⅰ has already reached 0.2 mm, and the maximum crack widths in Regions Ⅱ, Ⅲ, and Ⅳ are approximately 0.15 mm, 0.1 mm, and 0.15 mm, respectively.

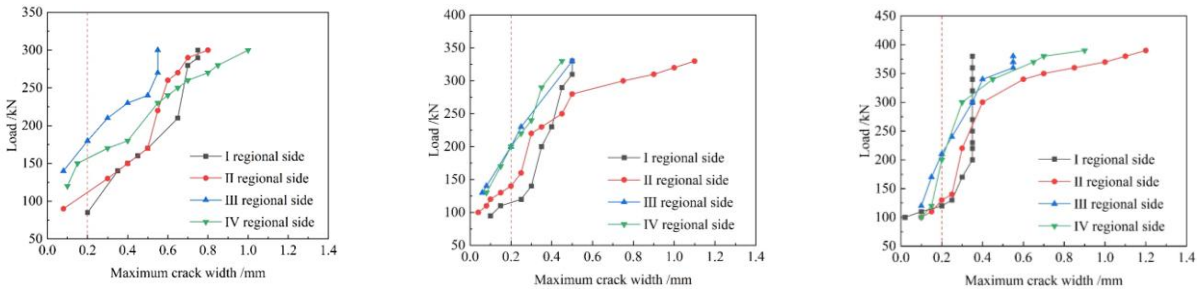

(a) – Beam B1 *(b) – Beam B2* *(c) – Beam B3*

Fig. 10 – Load-maximum crack width curves for beams B1, B2 and B3

The comparison of load-maximum crack width curves for Regions Ⅰ, Ⅱ, Ⅲ, and Ⅳ is presented in Figure 11. From Figure 11(a), it is evident that when the load is less than 150 kN, the maximum crack widths in Region Ⅰ of beams B1, B2, and B3 continuously increase with the rising load. However, when the load exceeds 150 kN, the crack widths grow at a relatively slower rate. At lower loads, the stiffness of the full normal concrete (NC) section is smaller than that of the UHPC-NC composite section, causing cracks to appear first in Region Ⅰ. As the load increases, both the number and width of these cracks expand. Once the load surpasses 150 kN, numerous cracks emerge at the vertical interface between the UHPC-NC composite section and the full NC section, as well as within the UHPC-NC composite section itself, leading to a significant reduction in the composite section's stiffness. Additionally, the bending moment in the composite section is greater than that in the outer full NC section, resulting in a less pronounced increase in maximum crack width in Region Ⅰ, while crack widths in other regions grow relatively faster.

From Figure 11(b), it can be observed that when the load is less than 150 kN or more than 280 kN, the crack width in Region Ⅱ of beams B1, B2, and B3 continuously increases with the rising load. However, when the load is between 150 kN and 280 kN, the crack width in Region Ⅱ changes insignificantly with the load. At loads below 150 kN, since Region Ⅱ is located at the vertical interface between the UHPC-NC composite section and the full NC section, the concrete there experiences a

larger bending moment than the outer full NC section, causing both Region Ⅱ and Region Ⅰ to crack earlier and exhibit faster crack width growth at lower loads. When the load exceeds 150 kN, numerous cracks appear in the UHPC-NC composite section, significantly reducing its stiffness. The bending moment in the composite section becomes larger than that at the vertical interface, resulting in a less pronounced increase in crack width in Region Ⅱ, while the crack width in the UHPC-NC composite section grows rapidly with the load. When the load exceeds 280 kN, the reinforcement in Region Ⅱ of beams B1, B2, and B3 yields or is about to yield, leading to a significant increase in crack width with the rising load.

From Figure 11(c), it can be seen that the load and crack width in Region Ⅲ of beams B1, B2, and B3 generally exhibit a linear relationship, with the crack width gradually decreasing as the reinforcement ratio increases under the same load. This is because, with an increased reinforcement ratio, more tensile stress is borne by the steel reinforcement under the same load, reducing the tensile stress borne by the UHPC and effectively suppressing the crack width in the UHPC-NC composite section.

From Figure 11(d), it is evident that the cracks in Region Ⅳ of beam B1 increase sharply with the rising load due to its lower reinforcement ratio, causing more tensile stresses to be borne by the UHPC as the load increases, leading to faster crack width development. In the pre-loading stage, the crack width growth in Region Ⅳ of beams B2 and B3 is relatively slow. However, when the load exceeds 300 kN, the crack width growth accelerates.

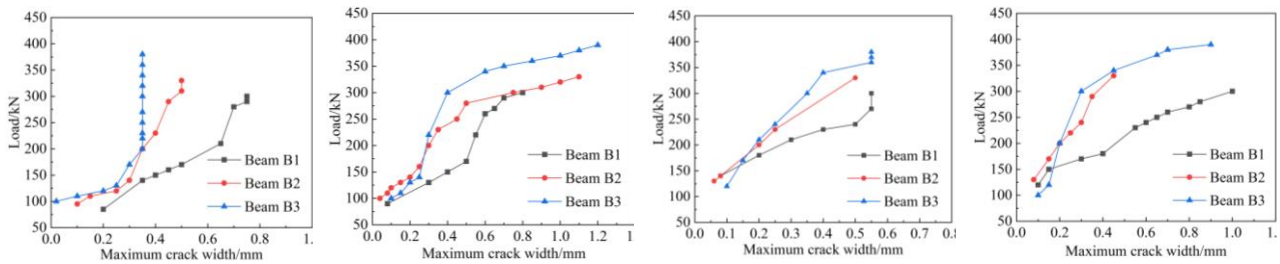

(a) – Region Ⅰ *(b) – Region Ⅱ* *(c) – Region Ⅲ* *(d) – Region Ⅳ*

Fig. 11 – Comparison of load-maximum crack width curves for regions Ⅰ, Ⅱ, Ⅲ and Ⅳ

UHPC Coverage Length Factors

The division of the test beam regions is illustrated in Figure 12. The variations in maximum crack width with respect to the applied load for each region of beams B4 and B5 are depicted in Figure 13. Additionally, a comparative analysis of the load versus maximum crack width curves for each region of the test beams is presented in Figure 14.

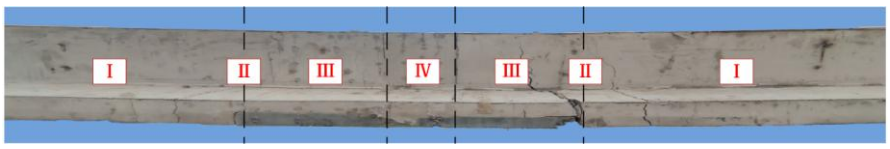

Fig. 12 – Map of the division of the test beam region (Beam B4)

As depicted in Figure 13(a), when beam B4 was loaded to 70 kN, cracks were observed in Region Ⅰ. As the load continued to increase, cracks successively appeared in Regions Ⅱ, Ⅲ, and Ⅳ. Upon reaching a load of 100 kN, the maximum crack width in Region Ⅰ was the first to reach 0.2 mm, while the maximum crack width in Region Ⅱ was 0.1 mm at that time; cracks had not yet appeared in Regions Ⅲ and Ⅳ. During the pre-loading stage, the crack widths in Regions Ⅰ and Ⅱ increased with the rising load. After loading reached 150 kN, cracks began to emerge in Regions Ⅲ and Ⅳ, and their widths increased accordingly with the load. However, the growth rate of crack

widths in Regions Ⅰ and Ⅱ became relatively slower. When the load exceeded 190 kN, the crack width in Region Ⅱ increased sharply with the rising load, ultimately leading to the failure of the test beam at the middle diaphragm section. After the load surpassed 240 kN, the crack width in Region Ⅰ also increased sharply with the rising load as part of the tensile reinforcement yielded.

From Figure 13(b), it can be observed that when beam B5 was loaded to 75 kN, cracks appeared in Region Ⅰ, followed by successive cracks in Regions Ⅱ, Ⅳ, and Ⅲ. When the load reached 110 kN, the maximum crack width in Region Ⅰ was the first to reach 0.2 mm, while the crack width in Region Ⅱ was 0.1 mm, and no cracks had appeared in Regions Ⅲ and Ⅳ. As the load continued to increase, the crack widths in all four regions generally exhibited linear growth. Notably, the crack widths in Regions Ⅲ and Ⅳ were similar and consistently smaller than those in Regions Ⅰ and Ⅱ. This was attributed to the "bridge-linking" effect of the steel fibers after the UHPC cracked, which effectively restricted the further development of the cracks. When the load exceeded 250 kN, the crack width in Region Ⅱ increased sharply with the rising load, ultimately leading to the failure of the test beam in this region.

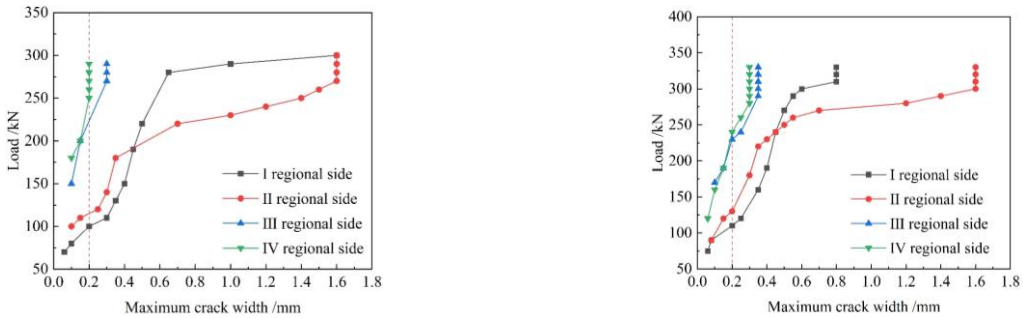

(a) – Beam B4 *(b) – Beam B5*

Fig. 13– Load-maximum crack width curves for beams B4 and B5

From Figure 14(a), it is evident that when the load is less than 150 kN, the crack widths in Region I of beams B2, B4, and B5 all increase with the rising load. However, when the load exceeds 150 kN, the rate of change in crack widths slows down. The crack width in the full NC section increases more gradually because cracks begin to appear in the UHPC-NC composite section at a load of 150 kN. Consequently, the crack widths in Regions Ⅲ and Ⅳ start to increase slowly with the increasing load, and the stiffness of the UHPC-NC composite section decreases significantly. As the load continues to rise, the crack width in Region I decreases with the increasing length of the UHPC-NC composite section. This is because a shorter UHPC-NC composite section results in a longer full NC section, which bears a larger bending moment. Additionally, the internal force redistribution in ordinary concrete is more pronounced, making it difficult to withstand larger bending moments. Therefore, under the same load, the crack widths in Region I of beams B4, B5, and B2 decrease in sequence. When the load exceeds 250 kN, the crack widths of beams B4 and B5 increase sharply with the rising load, while the crack width of beam B2 does not change significantly. This is because, at this point, the reinforcement in Region I of beams B2, B4, and B5 has already yielded or is about to yield, and more tensile stresses are borne by the UHPC. However, the cross-section of the UHPC-NC composite in beams B4 and B5 is shorter, leading to more steel fibers being extracted from the matrix.

From Figure 14(b), it can be observed that when the load is less than 150 kN, the crack widths in Region II of beams B2, B4, and B5 continuously increase with the rising load. This is because the bending moments at the vertical interface between the UHPC-NC and the full NC cross-sections are larger than those at the full NC cross-section, causing both Region II and Region I to crack earlier, and the crack widths to increase relatively rapidly during the preloading period. After the load exceeds 150 kN, with the decreasing stiffness of the UHPC-NC composite section, the crack

width in Region II increases relatively slowly. From Figures 14(c) and 14(d), it can be seen that the crack widths in Regions III and IV of beams B2, B4, and B5 generally increase linearly with the rising load. When the load exceeds 250 kN, the crack widths of beams B4 and B5 basically remain unchanged with the increasing load, while the crack widths of beam B2 continue to grow linearly.

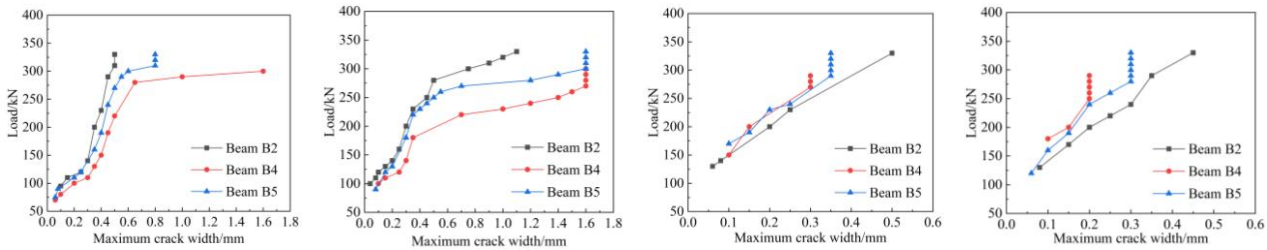

(a) – Region Ⅰ *(b) – Region Ⅱ* *(c) – Region Ⅲ* *(d) – Region Ⅳ*

Fig. 14 – Comparison of load-maximum crack width curves for regions Ⅰ, Ⅱ, Ⅲ and Ⅳ

UHPC Thickness and Form of Support

The division of the test beam regions is shown in Figure 15. The variation of maximum crack width with load in each region of beams B7 and B8 under load is shown in Figure 16, and the comparison of load-maximum crack width curves in each region of the test beams is shown in Figure 17.

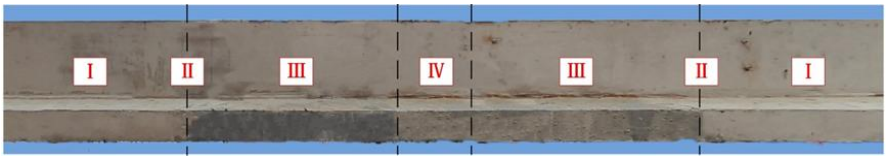

Fig. 15 – Map of the division of the test beam region (Beam B8)

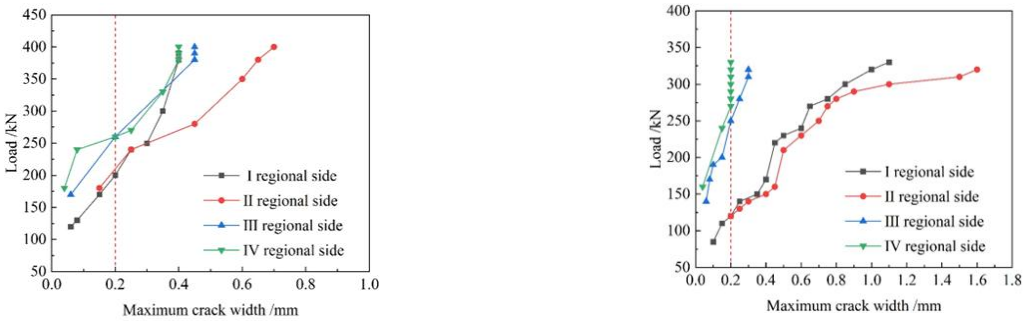

(a) – Beam B7 *(b) – Beam B8*

Fig. 16 – Load-maximum crack width curves for beams B7 and B8

As illustrated in Figure 18(a), the first crack emerged in Region Ⅰ when beam B7 was loaded to 120 kN. Subsequently, with the continuous increase in load, cracks successively appeared in Regions Ⅲ, Ⅱ, and Ⅳ. When the load reached 200 kN, the crack width in Region Ⅰ was the first to attain 0.2 mm, while the crack widths in Regions Ⅱ, Ⅲ, and Ⅳ were 0.15 mm, 0.1 mm, and 0.05 mm, respectively. As the load continued to rise, the crack widths in each region generally increased linearly, with those in Regions Ⅰ and Ⅱ being larger than those in Regions Ⅲ and Ⅳ.

From Figure 18(b), it can be observed that when beam B8 was loaded to 85 kN, cracks appeared in Region Ⅰ. As the load increased, cracks subsequently emerged in Regions Ⅱ, Ⅲ, and

Ⅳ in turn. When the load reached 120 kN, the crack widths in Regions Ⅰ and Ⅱ simultaneously reached 0.2 mm, while no cracks had yet appeared in Regions Ⅲ and Ⅳ. During the early stage of loading, the crack widths in Regions Ⅰ and Ⅱ grew with the increasing load. When the load exceeded 150 kN, as the crack widths in Regions Ⅲ and Ⅳ began to increase, the cross-sectional stiffness of the UHPC-NC composite section decreased, leading to a relatively steeper slope in the load-crack width curves for Regions Ⅰ and Ⅱ. When the load surpassed 290 kN, the crack widths in Regions Ⅲ and Ⅳ essentially remained unchanged, while some of the reinforcement in Regions Ⅰ and Ⅱ had yielded, resulting in a sharp increase in crack width at the section with the rising load. Ultimately, the test beam failed at the vertical interface between the UHPC-NC composite section and the full NC section.

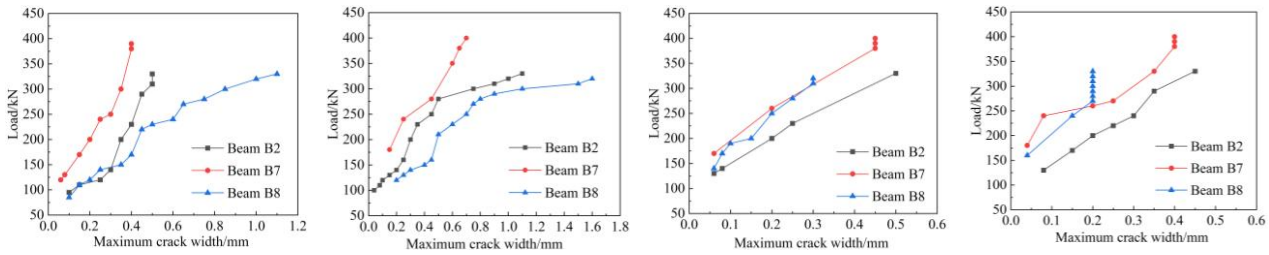

(a) – Region Ⅰ *(b) – Region Ⅱ* *(c) – Region Ⅲ* *(d) – Region Ⅳ*

Fig. 17 – Comparison of load-maximum crack width curves for regions Ⅰ, Ⅱ, Ⅲ and Ⅳ

From Figure 17(a), it is evident that as the load increases, the crack width in Region Ⅰ of beam B7 exhibits linear growth. Moreover, under the same load, the crack width in this region is smaller than that of beam B8. This is because the UHPC underlay enhances the flexural stiffness of the test beams, effectively suppressing crack development in Region Ⅰ. When the load is less than 150 kN, the crack widths in Region Ⅰ of beams B2 and B8 are similar, both increasing with the rising load. However, when the load exceeds 150 kN, the growth rate of crack width slows down. Under the same load, the crack width of beam B2 is smaller than that of beam B8.

At the early stage of loading, the stiffness of the full NC section is relatively low, causing the crack width in Region Ⅰ to develop more rapidly. When the load surpasses 150 kN, as the crack width in the UHPC-NC composite section increases, its sectional stiffness decreases. Coupled with the larger bending moment in the UHPC-NC composite section, the crack widths in Regions Ⅲ and Ⅳ grow faster, resulting in a relatively slower growth rate of crack width in Region Ⅰ. The thickness of the UHPC layer in beam B8 is greater than that in beam B2, providing a higher degree of steel fiber bridging. Consequently, the stiffness of the UHPC-NC composite section in beam B8 decreases more slowly, leading to smaller crack widths compared to beam B2. Furthermore, the decrease in cross-sectional stiffness is slower, and the crack widths and number of cracks in Regions Ⅲ and Ⅳ grow at a slower rate than in beam B2. Therefore, under the same loading conditions, the crack width in Region Ⅰ of beam B2 is smaller than that of beam B8.

From Figure 17(b), it can be observed that the crack width in Region II of beam B7 increases linearly with the rising load. Under the same load, the crack width of beam B7 is smaller than that of beam B8 because the UHPC underlay enhances the flexural stiffness of the test beams, effectively suppressing crack development in Region II. When the load is less than 150 kN, the crack widths of beams B2 and B8 increase with the load due to the larger bending moment at the vertical interface between the UHPC-NC composite section and the full NC section compared to the full NC section alone. Consequently, cracks in both Region Ⅱ and Region Ⅰ appear earlier, and the crack widths develop more rapidly.

From Figure 17(c), it is apparent that as the load increases, the crack widths in Region III of beams B7 and B8 are generally similar and both are smaller than that of beam B2 under the same load. This is because with the increase in UHPC thickness, the degree of bridging provided by steel fibers becomes greater, and its crack-arresting effect is more pronounced. From Figure 17(d), it can be seen that when the load is less than 270 kN, the crack widths in Region Ⅳ of beams B7 and B8 are similar and both are smaller than that of beam B2 under the same load.

Analysis of Maximum Crack Width in Pure Bending Zone

Reinforcement Ratio

Beams B1, B2, and B3 were tested to compare the effects of different reinforcement rates—0.36%, 0.43%, and 0.5%, respectively—on the flexural performance of a UHPC-strengthened simply-supported-to-continuous concrete box beam in the negative moment region. As illustrated in Figure 18, with an increase in the reinforcement rate, the cracking load of the UHPC-locally-reinforced simply-supported-to-continuous concrete box beam increased by 11.8% and 17.6%, the yield load rose by 17.4% and 47.8%, and the ultimate load increased by 14.8% and 28.5%. For the same reinforcement rate, the cracking load, yield load, and ultimate load of beam B2 increased by 46%, 12.5%, and 25%, respectively, compared to those of beam B0. Moreover, when the crack width in the purely curved section of beam B0 reached 0.2 mm, the crack width in beam B2 was only 0.1 mm.

The analysis revealed that reinforcing the negative moment zone of simply-supported-to-continuous concrete box beams with UHPC significantly enhanced the flexural performance of the test beams. As the reinforcement rate increased, the load-carrying capacity, stiffness, and ductility of the test beams improved markedly, and all test beams experienced damage at the intermediate diaphragm section. Compared to beam B0, the cracking load, yield load, and ultimate load of beam B6 increased by 38%, 4%, and 21%, respectively. When the maximum crack width in the purely curved section of beam B0 reached 0.2 mm, the crack width in beam B6 was 0.15 mm, which was closer to that of beam B2. This indicates that beam B2, which features UHPC reinforcement with a length of 1600 mm and a thickness of 60 mm, demonstrates comparable load-carrying and crack-limiting capabilities to a simply-supported-to-continuous prestressed concrete box beam reinforced with two additional prestressing strands of diameter 15.2 mm (with a tensile stress of 1000 MPa).

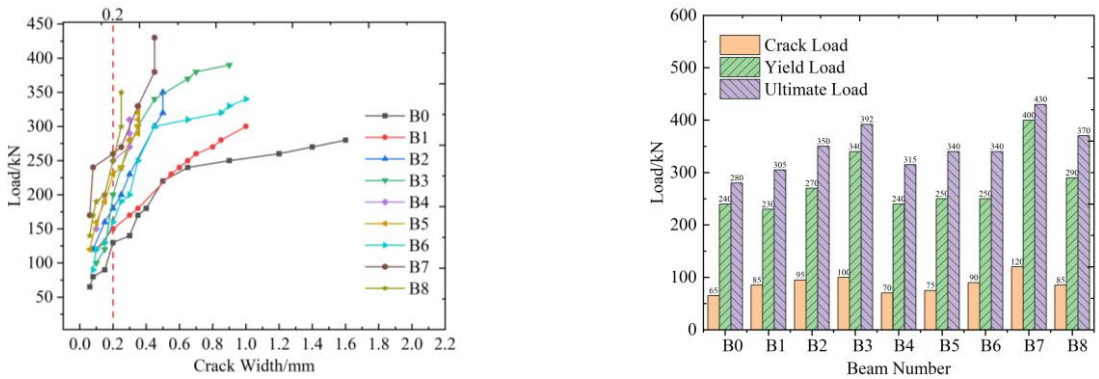

(a) – Load-maximum crack width curve for purely curved section

(b) – Eigenvalues of loads

Fig. 18 – Different reinforcement rates, UHPC lengths, UHPC thicknesses and support forms

UHPC Length

Beams B2, B4, and B5 were primarily tested to investigate the influence of varying UHPC cover lengths on the bending performance of UHPC-strengthened simply-supported-to-continuous concrete box beams in the negative moment zone. As depicted in Figure 18, when the UHPC cover

lengths were 1600 mm, 800 mm, and 1200 mm, the cracking load of the UHPC-locally-strengthened simply-supported-to-continuous concrete box beams increased by 46%, 7.7%, and 15%, respectively, compared to the control beam. The yield load increased by 12.5%, 0%, and 4%, while the ultimate load rose by 25%, 12.5%, and 21%, respectively. These results indicate that an adequate UHPC cover length is crucial, as shorter cover lengths result in less pronounced improvements in cracking load, yield load, and ultimate load.

When the crack width in the pure bending section of beam B0 reached 0.2 mm, the crack widths in beams B2, B4, and B5 were 0.1 mm, 0 mm, and 0.08 mm, respectively. This discrepancy can be attributed to the shorter cross-sectional lengths of the UHPC-NC combinations in beams B4 and B5, which caused a greater proportion of the external loads to be borne by the full NC section, thereby reducing the crack width in the pure bending section.

UHPC Thickness and Form of Support

Beams B2, B7, and B8 were primarily examined to explore the impact of varying UHPC thicknesses and bearing methods on the bending performance of UHPC-strengthened simply-supported-to-continuous concrete box beams in the negative moment zone. As illustrated in Figure 18, the cracking loads of UHPC-locally-strengthened simply-supported-to-continuous concrete box beams with UHPC thicknesses of 60 mm, 120 mm (with load bearing underneath the UHPC), and 120 mm (without specific load-bearing mention, assumed standard configuration) were 46%, 84.6%, and 30% higher, respectively, than those of the comparison beams. The yield loads were 12.5%, 66.7%, and 20.8% higher, while the ultimate loads were 25%, 53.6%, and 32% higher, respectively, compared to the comparison beams.

When the maximum crack width in the pure bending section of beam B0 reached 0.2 mm, the crack widths in beams B2, B7, and B8 were 0.1 mm, 0 mm, and 0 mm, respectively. The analysis revealed that UHPC with load bearing underneath significantly enhanced the stiffness, load-carrying capacity, and crack-controlling ability of the test beams. However, under larger loads, the UHPC in the tensile zone of beam B7 entered the stress-softening stage, and the steel fiber "bridging" effect was not as pronounced as in beam B2 (assuming the comparison was intended to be with B2 or another relevant beam; if not, please adjust accordingly).

CONCLUSION

1. When the crack width in the pure bending section of a plain reinforced concrete box beam reaches 0.2 mm under the same reinforcement ratio, the crack width in a UHPC-reinforced beam is only 0.1 mm. Reinforcing the negative moment zone of a simply-supported-to-continuous concrete box beam with UHPC can significantly enhance the cracking performance of the test beam. When the UHPC length is small, a greater portion of the external loads is borne by the full NC (normal concrete) section, resulting in a smaller crack width in the pure bending section. Therefore, to achieve optimal crack resistance, it is essential to ensure an adequate UHPC length.
2. The reinforced beams were categorized into four regions: the full NC section, the vertical interface between the UHPC-NC combined section and the full NC section, the UHPC-NC combined section, and the intermediate diaphragm section. The crack development patterns in each region of the test beams were systematically analyzed under varying reinforcement rates, UHPC lengths, and UHPC thicknesses. The analyses revealed the following:

(1) As the UHPC length increases, the maximum crack width at the vertical interface between the full NC section and the UHPC-NC combined section, as well as within the full NC section itself, decreases significantly. However, the crack width at the UHPC-NC combined section and the intermediate diaphragm section increases slightly. When the UHPC length is relatively small, its crack-limiting ability is not pronounced, showing performance similar to that of the comparison beams.
(2) Increasing the thickness of the UHPC leads to a significant reduction in the maximum crack width at the UHPC-NC combined section and the intermediate diaphragm section. Conversely, the

crack width at the vertical interface between the UHPC-NC combined section and the full NC section increases notably.

(3) When the reinforcement ratio of ordinary steel bars is the same, beam B2 demonstrates superior crack-limiting ability compared to beam B0. Specifically, when the crack width in the pure bending section of beam B0 reaches 0.2 mm, that of beam B2 is only 0.1 mm. Furthermore, the crack width in the pure bending section of a simply-supported-to-continuous prestressed concrete box beam reinforced with two additional 15.2-diameter prestressing strands is 0.15 mm, indicating comparable performance between beams B2 and B6.

REFERENCES

[1] Hu Tie - ming, He Cheng - kui, Chen Xiao - feng, et al., 2010. Fatigue experiment of concrete bridges strengthened by simple - supporting to continuous construction method. China Journal of Highway and Transport, vol. 23, p. 76. https://doi.org/10.19721/j.cnki.1001-7372.2010.05.012.

[2] Nielson B G, DesRoches R., 2007. Seismic performance assessment of simply supported and continuous multispan concrete girder highway bridges. Journal of Bridge Engineering, vol. 12, p. 611 - 620. https://doi.org/10.1061/(ASCE)1084-0702(2007)12:5(611)

[3] Arrayago I, Real E., 2016. Experimental study on ferritic stainless steel simply supported and continuous beams. Journal of Constructional Steel Research, vol. 119, p. 50 - 62. https://doi.org/10.1016/j.jcsr.2015.12.006

[4] Mohamed A M, Mahmoud K, El - Salakawy E F., 2020. Behavior of simply supported and continuous concrete deep beams reinforced with GFRP bars. Journal of Composites for Construction, vol. 24, p. 04020032. https://doi.org/10.1061/(ASCE)CC.1943-5614.0001039

[5] Sun Q, Yang Y, Fan J, et al., 2014. Effect of longitudinal reinforcement and prestressing on stiffness of composite beams under hogging moments. Journal of Constructional Steel Research, vol. 100, p. 1 - 11. https://doi.org/10.1016/j.jcsr.2014.04.017

[6] Su Q, Yang G, Bradford M A., 2015. Behavior of a continuous composite box girder with a prefabricated prestressed - concrete slab in its hogging - moment region. Journal of Bridge Engineering, vol. 20, p. B4014004. https://doi.org/10.1061/(ASCE)BE.1943-5592.0000698

[7] Chen S., 2005. Experimental study of prestressed steel–concrete composite beams with external tendons for negative moments. Journal of Constructional Steel Research, vol. 61, p. 1613 - 1630. https://doi.org/10.1016/j.jcsr.2005.05.005 https://doi.org/10.1016/j.jcsr.2005.05.005

[8] Gong W, Li X, Ge Z, et al., 2023. Steel - concrete composite beams strengthened with NSM CFRP systems at the hogging - moment regions. Engineering Structures, vol. 292, p. 116576. https://doi.org/10.1016/j.engstruct.2023.116576

[9] Liu X, Tang L, Jing Y, et al., 2022. Behaviour of continuous steel–concrete composite beams strengthened with CFRP sheets at hogging - moment region. Composite Structures, vol. 291, p. 115695. https://doi.org/10.1016/j.compstruct.2022.115695

[10] Maghsoudi A A, Bengar H A., 2009. Moment redistribution and ductility of RHSC continuous beams strengthened with CFRP. Turkish Journal of Engineering & Environmental Sciences, vol. 33, p. 1. https://doi.org/10.3906/MUH-0901-6

[11] Abdullah A Q, Mansor A A, Mohammed A S, et al., 2021. Hybrid and external strengthening of T - reinforced concrete beams under negative bending moment using steel plates and CFRP. IOP Conference Series: Earth and Environmental Science, vol. 856, p. 012027. https://doi.org/10.1088/1755-1315/856/1/012027

[12] Gholamhoseini A, Khanlou A, MacRae G, et al., 2018. Short - term behaviour of reinforced and steel fibre–reinforced concrete composite slabs with steel decking under negative bending moment. Advances in Structural Engineering, vol. 21, p. 1288 - 1301. https://doi.org/10.1177/1369433217739710

[13] Liu R, Yang Y, Zhou X., 2018. Experimental study on fatigue performance of composite beam with steel - plate - concrete composite decks. Construction and Building Materials, vol. 188, p. 833 - 849. https://doi.org/10.1016/j.conbuildmat.2018.08.108

[14] Ibrahim A, Salem S, Khalil A, et al., 2020. Experimental Investigation for Moment Redistribution in Continuous RC Beams Top Strengthened with CFRP and Steel Plates. IOP Conference Series: Materials Science and Engineering, vol. 809, p. 012007. https://doi.org/10.1088/1757-899X/809/1/012007

[15] Lin W, Yoda T, Taniguchi N, et al., 2014. Mechanical performance of steel - concrete composite beams subjected to a hogging moment. Journal of Structural Engineering, vol. 140, p. 04013031. https://doi.org/10.1061/(ASCE)ST.1943-541X.0000800

[16] Russell H G, Graybeal B A, Russell H G., 2013. Ultra - high performance concrete: A state - of - the - art report for the bridge community. United States. Federal Highway Administration. Office of Infrastructure Research and Development.

[17] Zhang P, Hu R, Zou X, et al., 2021. Experimental study of a novel continuous FRP - UHPC hybrid beam. Composite Structures, vol. 261, p. 113329. https://doi.org/10.1016/j.compstruct.2020.113329

[18] Long G, Zhou R, Ma H, et al., 2022. Experimental and Numerical Study on UHPC–RC Decks within Hogging Moment Region. Applied Sciences, vol. 12, p. 11446. https://doi.org/10.3390/app122211446

[19] Liu X, Zhang J, Cheng Z, et al., 2021. Experimental and numerical studies on the negative flexural behavior of steel - UHPC composite beams. Advances in Civil Engineering, vol. 2021, p. 1 - 15. https://doi.org/10.1155/2021/8828175

[20] Wan Z, Fang Z, Liang L, et al., 2022. Structural performance of steel–concrete composite beams with UHPC overlays under hogging moment. Engineering Structures, vol. 270, p. 114866. https://doi.org/10.1016/j.engstruct.2022.114866